Journal of Materials Chemistry A

ROYAL SOCIETY OF CHEMISTRY

PAPER

View Article Online
View Journal | View Issue

Cite this: J. Mater. Chem. A, 2025, 13, 33832

Poly(ether-imide-ester)s incorporating sulfur-containing amino acids: a first step toward more sustainable high-dielectric polymer materials

Sebastian Bonardd, *[a] Maksim Bratukhin,[bc] Federico Guerrero-Ruiz,[a] Sara Zanchi, [d] Florian Le Goupil, [d] David Díaz Díaz, [bc] José A. Pomposo [aef] and Jon Maiz *[ae]

The development of high-dielectric polymer materials is critical for advancing energy storage and conversion technologies. In this study, we report the synthesis and characterization of novel poly(ether-imide-ester) (PEIE) polymers incorporating sulfur-based amino acid residues as dipolar units. Specifically, we designed and synthesized two PEIEs containing methionine (PEIE-Met) and its oxidized form, methionine sulfone (PEIE-Met(O_2)), to investigate the impact of pendant thioether and sulfone groups on the dielectric properties. The synthesized polymers were thoroughly characterized *via* spectroscopic (FTIR, NMR), thermal (TGA, DSC), and dielectric (BDS) techniques. The results confirm the successful incorporation of methionine-based moieties into the polymer backbone, leading to the formation of materials showing high thermal stability, as evidenced by onset degradation temperatures above 300 °C, glass transition temperatures (T_g) in the 162–182 °C range, and excellent dielectric performance. Notably, at room temperature, PEIE-Met(O_2) exhibited a higher dielectric constant ($\varepsilon_r' = 7.1$ at 1 Hz) than PEIE-Met did ($\varepsilon_r' = 5.7$ at 1 Hz), which was attributed to the increased dipole moment of the sulfone groups. Both polymers maintained low dielectric loss values (tan(δ) < 0.01) at room temperature, making them promising candidates for capacitor applications. Notably, the materials developed in this work exhibited discharge efficiency values above 85% at 100 °C under electric fields of 100 and 200 MV m^{-1}, confirming their suitability as dielectric layers for energy storage applications. This study highlights the potential of bioderived amino acid residues as functional building blocks for high-dielectric polymer design. Our findings open new avenues for the development of sustainable, high-performance dielectric materials tailored for next-generation electronic and energy storage applications.

Received 8th April 2025
Accepted 27th August 2025

DOI: 10.1039/d5ta02785c

rsc.li/materials-a

1. Introduction

In the last decade, the field of polymer dielectrics has gained significant attention from the scientific community. This is unsurprising given the broad range of electrical applications where these materials are used, especially those related to energy storage and conversion systems, which are considered crucial owing to our current society's energy landscape.[1,2] In this context, capacitor technologies have notably benefited from the development of more efficient polymer dielectrics, which have increased the use and performance of these devices in various high-tech applications, such as power-pulse electronics, accumulators in renewable energy farms, hybrid/electrical means of transportation, aerospace technology, robotics, and sensors.[2–6] However, the use of capacitors is not restricted solely to high-tech fields, as they also find a fundamental place in most of the trivial circuitry that surrounds us daily, ensuring the proper functioning of household appliances, defibrillators and many other essential devices.

As dielectric materials, compared with their inorganic counterparts, polymers have several advantages that make them excellent candidates for the manufacture of capacitor devices. In this context, polymers have become the preferred option due to their inherent insulating nature, high dielectric breakdown values (E_b), excellent mechanical properties, easy processing, light weight, chemical resistance, synthetic versatility, and cost-effective production.[2,7,8] However, one of the main drawbacks in this matter is the low dielectric constant (ε_r') that they tend to

[a]Centro de Física de Materiales (CFM-MPC), CSIC-UPV/EHU, Paseo Manuel de Lardizábal 5, 20018 Donostia-San Sebastián, Spain. E-mail: sebastianignacio.bonardd@ehu.eus; jon.maizs@ehu.eus

[b]Departamento de Química Orgánica, Universidad de La Laguna, Avda. Astrofísico Francisco Sánchez 3, La Laguna 38206, Tenerife, Spain

[c]Instituto Universitario de Bio-Orgánica Antonio González, Universidad de La Laguna, Avda. Astrofísico Francisco Sánchez 2, La Laguna 38206, Tenerife, Spain

[d]Univ. Bordeaux, CNRS, Bordeaux INP, LCPO, UMR 5629, F-33600, Pessac, France

[e]IKERBASQUE – Basque Foundation for Science, Plaza Euskadi 5, 48009, Bilbao, Spain

[f]Departamento de Polímeros y Materiales Avanzados: Física, Química y Tecnología, Universidad del País Vasco-Euskal Herriko Unibertsitatea (UPV/EHU), Paseo Manuel de Lardizábal 3, 20018, Donostia-San Sebastián, Spain

exhibit, which usually falls in the range of 2.0–4.0.[6] This is a critical aspect when considering that both the capacitance ($C_p = (\varepsilon_r' \varepsilon_o A)/d$, with ε_o, A and d being the vacuum permittivity, the electrode's area and the thickness of the dielectric layer, respectively) and discharged energy density ($U_e = 1/2\varepsilon_r' \varepsilon_o E^2$, with E being the applied electric field) of a capacitor depend directly on this parameter.[7] The above has triggered the search for new strategies to prepare high-dielectric polymers, a term coined for those systems with ε_r' values above 5.0, which, considering all the progress made to date, can be established as the benchmark value to overcome.[2] In this regard, the dipolar glass polymer (DGP) concept introduced by Lei Zhu in 2014 has managed to maintain its status as one of the most efficient strategies for generating high-dielectric polymers that also present low dissipative behavior.[6] The latter is also relevant in regard to energy storage applications.

In its simplest definition, a DGP must fulfill two main conditions. First, to count with small-sized high dipole moment functional groups covalently attached to its structure, and second, to be an amorphous material with the highest possible glass transition temperature (T_g). Thus, the high ε_r' achieved by these materials results from their improved ability to be polarized, which is ascribed to the orientational motions that these molecular dipoles can pursue within the free volume provided by the amorphous matrix when exposed to an external electric field. On the other hand, the high T_g requirement is supported by the exalted dissipative behavior that these materials exhibit when they enter the rubbery state as a result of approaching or surpassing their T_g. In this sense, the enhanced mobility of polymer chains unlocks well-known dissipative phenomena, such as long-range segmental relaxations, which introduce molecular friction along with the appearance of ionic conductivity caused by the increased diffusion of ionic impurities. Moreover, from a device perspective, if the working temperature is close to or above the T_g, the material may lose mechanical stability, favoring its drainage out of the device and inducing its failure. Therefore, the ideal picture of a DGP would be a material bearing molecular dipoles able to move at very low temperatures (through so-called sub-T_g transitions) within a high-T_g vitreous matrix. This allows the system to work over a wide range of temperatures presenting enhanced polarization and low dissipative character, resulting in a high ε_r' and a reasonably low loss factor (tan(δ)).

Taking this into account, the current state of the art has proven that sulfones have emerged as the best candidates for designing DGPs when choosing dipolar structures. In a pioneering manner, Wei *et al.* were the first to report a DGP containing sulfonyl groups, achieving outstanding values of 11.4 and 0.02 (at 1 Hz, 25 °C) for ε_r' and tan(δ), respectively.[9] From that on, the superiority of these entities has been confirmed through numerous reports on sulfonyl-containing polymers that have managed to significantly outperform the performance of conventional polymeric systems.[10–17] Our group has contributed to these findings by studying diverse polymer-based systems bearing these types of entities and comparing them with other well-known and widely employed candidates, such as nitriles.[18,19] In all the cases, we confirmed through experimental and theoretical approaches that sulfones allow the preparation of DGPs with remarkably high ε_r' values. The above might find answer not only in the high dipole moment of these structures but also in their apparent increased mobility within polymer matrices, facilitating their orientational motions and, consequently, improving the material's polarization. However, the inclusion of these molecular structures into different polymer backbones is not always an easy task; occasionally, low-yield chemical protocols that involve the use of toxic and non-easy-to-handle substrates are needed. On the other hand, several strategies have been adopted in regard to preparing high-T_g DGPs. For example, the covalent incorporation of bulky/rigid structures as pendant groups and the elaboration of covalently crosslinked polymer networks have become suitable strategies to prepare high-T_g materials with good resistance to high external voltages.[20–23] Furthermore, the use of rigid and twisted dipolar monomeric units has been tested in the preparation of DGPs with intrinsic porosity to achieve high-temperature-tolerant materials with adequate dipolar mobility.[24,25] Recently, our group pioneered the development of the dipolar glass copolymer concept as a strategy to increase the T_g of DGPs by incorporating dipolar comonomers that confer rigidity to the polymer backbone without negatively impacting the system's polarization.[26,27] Nevertheless, one of the most effective and straightforward strategies for elaborating high-T_g DGPs has always been the manufacture of polymeric structures having a high aromatic content, especially in the main chain.[28,29] Excellent examples of the above are polycondensates such as poly(ethers), poly(imide)s and poly(carbonate)s, which have shown adequate features as dielectric materials for high-temperature applications, particularly referring to T_g and tan(δ) values.[29–37] Unfortunately, although few reports exist, obtaining this class of polymers with high ε_r' values has never been easy, even after the incorporation of high-dipole functional groups. A feasible explanation for the above is the notably low dipole density that these materials tend to exhibit because of their high monomeric molecular mass.[21] Thus, the incorporation of multiple dipolar entities into aromatic monomer structures is an interesting approach to solve the above-mentioned issue.

Towards this end, a quick survey of the literature allows the discovery of poly(ether-imide-ester)s (PEIEs).[38,39] These polycondensates are distinguished by their variety in terms of chemical structure, with monomeric structures built and subsequently polymerized from various molecular fragments linked together through ether, imide and ester bonds. In this context, PEIEs offer the possibility of being designed to match the required properties for a wide range of applications, allowing them to be classified as high-performance polymer materials.[40] From our perspective, aromatic PEIEs have emerged as interesting candidates for assessing the preparation of high-T_g DGPs since they already have a backbone nourished by multiple molecular dipoles (*e.g.*, carbonyl species). However, the dipolar contribution of these systems could be further increased by the rational design of monomer structures containing additional dipole entities, ideally sulfones. Thus, while seeking strategies to incorporate sulfones into PEIEs, we

realized that several amino acids, including methionine, have been used as building blocks in the confection of PEIEs and other similar polycondensates.[39,41–43] In this context, methionine is ideal for this purpose since its thioether unit can be easily oxidized into sulfone, leading to the preparation of methionine sulfone, which, fortunately, is also commercially available.[44] To our surprise, the use of methionine as a source of sulfones in the synthesis of polymer dielectrics has never been explored, and we find particular motivation in introducing to this field the use of this class of bioderived moieties, which nature has already synthesized for us.

The present work is motivated by the exploration of amino acid fragments for designing high-dielectric polymer materials, aligning with our current needs to transition away from fossil-derived components and supporting new strategies for advancing sustainability in materials science. In this sense, using these bio-based and non-petroleum-derived building blocks has garnered significant attention for developing sustainable materials across various research fields, largely due to their structural diversity and versatile properties. Through this strategy, we aimed to provide a new alternative for introducing the essential sulfone groups into polymer structures, which are renowned chemical entities that play a crucial role in achieving exceptionally high dielectric constants in dipolar glass polymers. Thus, from a sustainable perspective, the gain from this approach is to circumvent the conventional synthetic routes typically required to obtain sulfones, which involve the oxidation of thioethers and mercaptans derived from the treatment of petrochemical sources. To this end, we synthesized and studied two different PEIEs, both thermally and dielectrically containing methionine and methionine sulfone, which serve as sources of high-dipole moment entities. To ensure an increased dipole density along with a high T_g value, the design of these specimens also considered the incorporation of aromatic high-dipole moment structures into their backbones. We hypothesize that incorporating thioether and sulfone units as pendant groups will enhance the polarization capacity of these materials because of their greater freedom of orientational motion. Furthermore, because of the significantly greater dipole moment of the sulfone groups, we also expect the samples containing these entities to exhibit improved dielectric properties.

2. Experimental section

2.1 Materials

Phtalimide (≥99%), 4,4′-sulfonyldiphenol (98%), D,L-methionine (>99%), D,L-methionine sulfone (>99%), nitric acid (HNO_3, 70%), sulfuric acid (H_2SO_4, 95–98%), hydrochloric acid (HCl, 37%), sodium hydroxide (NaOH, ≥99%), potassium hydroxide (KOH, ≥99%), ammonium chloride (NH_4Cl, ≥99.5%) and thionyl chloride ($SOCl_2$, 97%) were purchased from Merck. Acetic acid (CH_3COOH, glacial), methanol (MeOH, 99.9% (GC)) and *N*,*N*′-dimethylformamide (DMF, ≥98.5%) were acquired from Sigma-Aldrich. D,L-Alanine (98.5%), *p*-toluenesulfonyl chloride (TsCl, >99%) and pyridine (Py, >99%) were purchased from TCI Chemical. All reagents and solvents used in this work were used without further purification unless otherwise stated.

2.2 Characterization techniques

^{1}H-NMR and ^{13}C-NMR spectra were recorded on a Bruker Avance II-500 system using DMSO-d_6 as the solvent for the monomers and polymers. Fourier transform infrared spectroscopy (FTIR) was carried out using a Jasco FT/IR – 6300 spectrophotometer. The spectra were recorded in the range of 500 to 4000 cm^{-1} after 34 scans in transmission mode with a resolution of 2 cm^{-1}. The samples were prepared as KBr pellets. The molecular weights of the polymers were determined *via* size-exclusion chromatography (SEC) *via* a Shimadzu Nexera 40 HPLC system equipped with a polar gel-M guard (50 × 7.5 mm) and a polar gel-M column (300 × 7.5 mm), both from Agilent. A differential refractive index (dRI) detector (RID-20A, Shimadzu) was used as a detection system. A solution of LiBr in *N*,*N*-dimethylformamide (DMF) (0.1 wt%) was used as the eluent at a flow rate of 1 mL min^{-1}, with polystyrene (PS) standards used for conventional calibration.

The thermal characterization of the samples was carried out *via* a simultaneous thermal analyzer (TG/DSC) Discovery SDT 650 (TA Instruments) and a differential scanning calorimeter Discovery DSC 025 (TA Instruments). Thermogravimetric analysis (TGA) was performed between 25 °C and 900 °C at 10 °C min^{-1} under a nitrogen atmosphere. From the obtained thermograms, the degradation onset temperature (T_i), maximum weight loss rate temperature (T_{MD}), and residue percentage (R) were calculated. T_i was defined as the temperature at which the material lost 5% of its initial weight. Differential scanning calorimetry (DSC) analysis consisted of the following five consecutive steps: (i) dynamic heating from 25 °C to 200 °C at 20 °C min^{-1}, (ii) isothermal process at 200 °C for 3 min, (iii) dynamic cooling process from 200 °C to 0 °C at 20 °C min^{-1}, (iv) isothermal process at 0 °C for 3 min, and finally, (v) a dynamic heating process from 0 °C to 230 °C at 10 °C min^{-1}. The reported glass transition temperatures (T_g) were calculated from the inflection point measured in thermograms acquired from the last heating step.

Broadband dielectric spectroscopy (BDS) was used to characterize the dielectric properties of the materials. Measurements were carried out *via* a Novocontrol Alpha high-resolution analyzer with an applied AC voltage of 1.0 V, from which frequency scans (isothermal spectra) and temperature scans (isochronal spectra) were obtained. Frequency scans were measured in the range between 10^{-1} and 10^5 Hz. These measurements were taken at different temperatures ranging from −150 °C to 50 °C. On the other hand, isochronal spectra were recorded from −150 °C to 150 °C at frequencies between 1 Hz and 10^6 Hz. The sample preparation for dielectric measurements is outlined below. First, a given amount of polymer powder was compressed at room temperature under 10 tons of pressure into a disc-shaped sample. The obtained sample was then hot-pressed between two Teflon discs at a temperature of T_g +30 °C and pressure of 2 bar for 45 min, resulting in the formation of a bubble-free homogeneous film.

This film was then hot-pressed again between two gold-plated electrodes of different diameters (10 mm and 20 mm), with the larger-diameter electrode used as the bottom part of the sandwich configuration. Initially, the thickness of the film was determined as the difference in thickness between both electrodes before and after hot pressing the polymer film. However, the above value was corrected by measuring the thickness of the film peeled off from the electrodes after the dielectric measurements. The samples placed between electrodes were dried overnight under vacuum at 150 °C and then stored in a desiccator before analysis. Dielectric constant values (ε_r') were calculated using eqn (1):

$$\varepsilon_r' = \frac{C_P' d}{\varepsilon_O \pi r^2} \quad (1)$$

where C_p' is the real part of the measured capacitance in the parallel configuration, d is the thickness of the polymer film, ε_o is the vacuum permittivity (8.85×10^{-12} F m^{-1}) and r is the radius of the top electrode. Once ε_r' was calculated, the dielectric loss (ε_r'') was determined *via* the relation $\varepsilon_r'' = \varepsilon_r' \tan(\delta)$, where $\tan(\delta)$ is the loss factor obtained directly from the experimental measurements.

Polarization *vs.* electric field loops (*P*–*E* loop) were measured on capacitors and recorded at room temperature using a TF Analyzer 2000E (aixACCT Systems). The measurements employed a continuous triangular wave with a frequency of 100 Hz, applying an electric field between 0 MV m^{-1} and 300 MV m^{-1}. The capacitors were fabricated with two gold electrodes separated by an active polymer layer, as detailed below. First, an 80 nm thick gold electrode was thermally evaporated onto a clean glass substrate using a ME400B PLASSYS evaporator. Solutions in cyclopentanone of the polymer of interest (250 mg mL^{-1}) were spin-coated onto the substrate at 1200 rpm for 60 seconds, resulting in films with thicknesses around 0.6–1.5 μm. Prior to the thermal evaporation of the top electrode, the samples underwent thermal treatments in vacuum to remove traces of solvent. Subsequently, a second 80 nm tick gold electrode was thermally evaporated. From *P*–*E* loops measurements the discharged energy density (U_e) and discharge efficiency (η) were calculated using eqn (2) and (3).[45]

$$U_e = \int_{D\,max}^{0} E \mathrm{d}D = \frac{1}{2}\varepsilon_O \varepsilon_r' E^2 \quad (2)$$

$$\eta = [U_e/(U_e - U_l)] \times 100 \quad (3)$$

Where D represents the dielectric displacement and U_l is the energy density lost during the discharge process.

3. Results and discussion

The first part of this work was devoted to preparing monomeric structures containing D/L-methionine and D/L-methionine sulfone residues, hereafter referred to as EIA-Met and EIA-Met(O_2), respectively. Both monomers were successfully synthesized *via* the multistep route illustrated in Scheme 1, which was designed on the basis of previous reports with slight variations when needed.[39,42] Starting from phthalimide (**1a**), mononitration of this substrate (**1b**), followed by imide ring

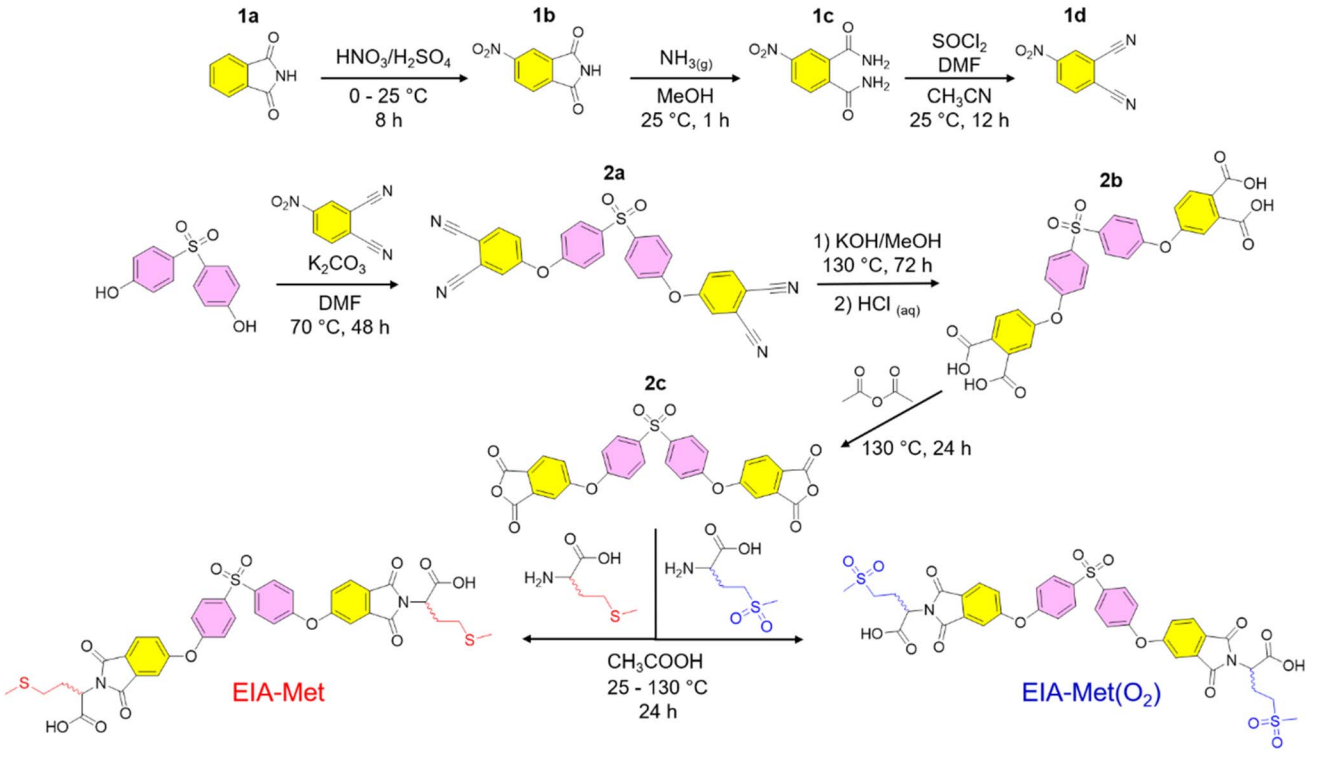

Scheme 1 Multistep synthetic route for the preparation of EIA-Met and EIA-Met(O_2) monomers.

opening *via* NH_3 gas, led to the formation of **1c**. The primary amides in **1c** then underwent dehydration using thionyl chloride and a catalytic amount of DMF, yielding 4-nitrophthalonitrile (**1d**). Two equivalents of this intermediate (**1d**) were coupled with one equivalent of 4,4′-sulfonyldiphenol, producing the tetranitrile derivative (**2a**), which was subsequently oxidized to the corresponding tetraacid (**2b**). Next, intramolecular condensation of the carboxylic acids in **2b** was promoted *via* acetic anhydride, leading to the formation of **2c**. Finally, EIA-Met and EIA-Met(O_2) were synthesized by incorporating the respective amino acids into **2c** *via* well-established thermal imidization protocols.[46] Overall, both monomers and their corresponding intermediates were obtained on a gram scale with good to excellent yields (>60%) and without the need for tedious purification protocols other than precipitation and washing steps. ^{1}H and ^{13}C-NMR confirmed the successful synthesis of the monomers and intermediates, with their spectra and synthetic protocols available in the SI.

Scheme 1 shows that both monomers have nearly identical chemical structures, differing only in the pendant group attached to the amino acid fragment. In this context, the monomer structures were designed to maximize the number of dipolar groups, thereby increasing the dipole density of the final polymers. Thus, the use of 4,4′-sulfonyl diphenol (pink) as a central building block in EIA-Met and EIA-Met(O_2), linked through ether bonds to phthalimides (yellow) containing the respective amino acid structures, proved to be an effective strategy for incorporating multiple high-dipole-moment functional groups. As depicted in Scheme 2, both monomers were polymerized separately, utilizing 4,4′-sulfonyl diphenol (green) as a comonomer *via* the Higashi method.[47] This method enables the synthesis of aromatic polyesters with high conversions while minimizing the elevated temperatures and long reaction times typically required by other conventional procedures. Additionally, as anticipated, the repeated use of 4,4′-sulfonyl diphenol during the polymerization process was conceived as a strategy to introduce additional sulfone dipoles, preserving the high-dipolar character of the polymer backbone. Both EIA-Met and EIA-Met(O_2) monomers were successfully polymerized, yielding fine brown powders, PEIE-Met and PEIE-Met(O_2), with conversion values of 93% and 95%, respectively (Scheme 2).

Fig. 1A shows the FTIR spectra recorded for the obtained materials. The high similarity between the two spectra results from the nearly identical chemical structures of both samples. Nevertheless, the subtle differences observed can be attributed to the single distinction between them: the nature of the pendant group in the amino acid fragment. The common signals identified in Fig. 1A include bands labeled 1 and 2 (~1775 and 1720 cm^{-1}), which arise from vibrational motions of carbonyl species forming parts of the imide and ester groups, respectively.[41,43] Then, at lower wavenumbers, signals 3 (1587 cm^{-1}) and 4 (1482 cm^{-1}) are assigned to C–C and C–O vibrations, where carbon atoms are part of aromatic structures. Vibrational band 5, appearing at 1383 cm^{-1}, is associated with linkage motions of the imide heterocycle, whereas signals 6 (1237 cm^{-1}) and 8 (1105 cm^{-1}) correspond to C–O–C structures in ether and ester groups along the main chain.[39,41]

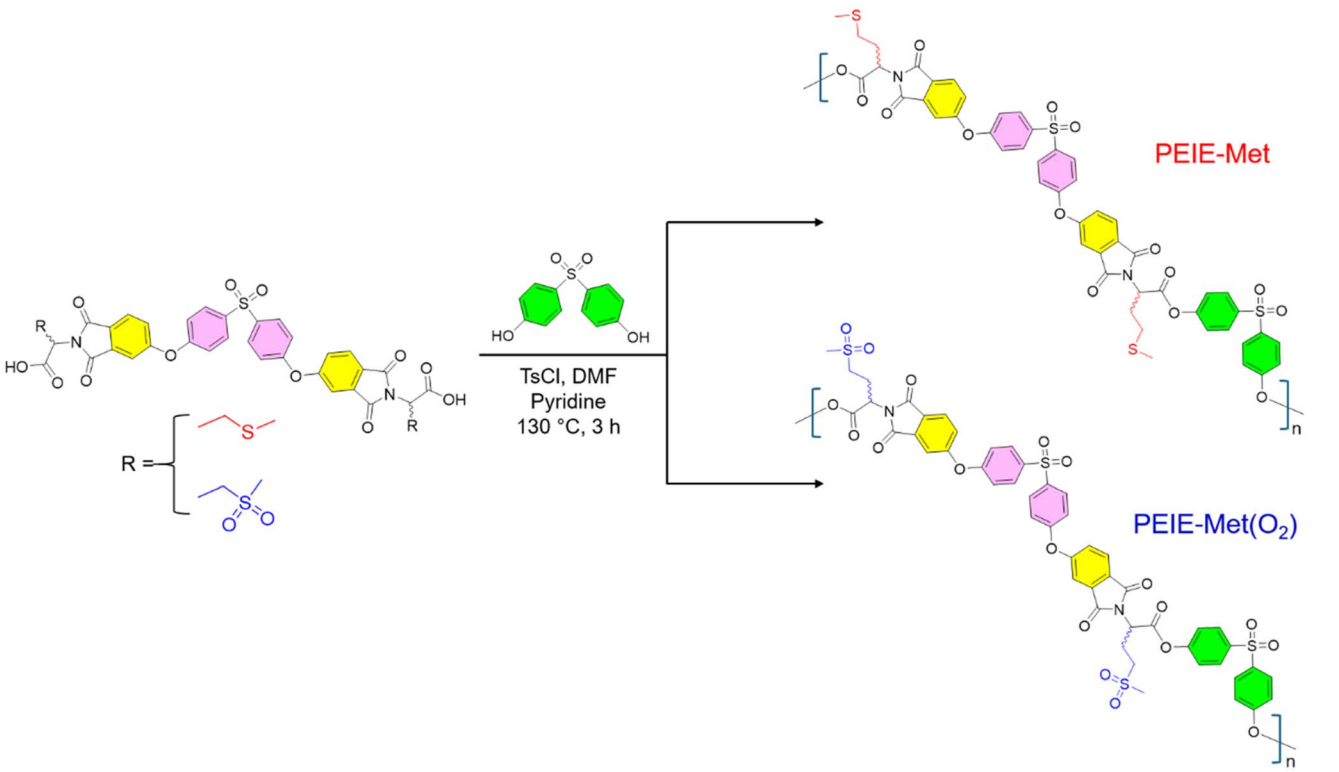

Scheme 2 Polymerization of EIA-Met and EIA-Met(O_2) *via* the Higashi method.

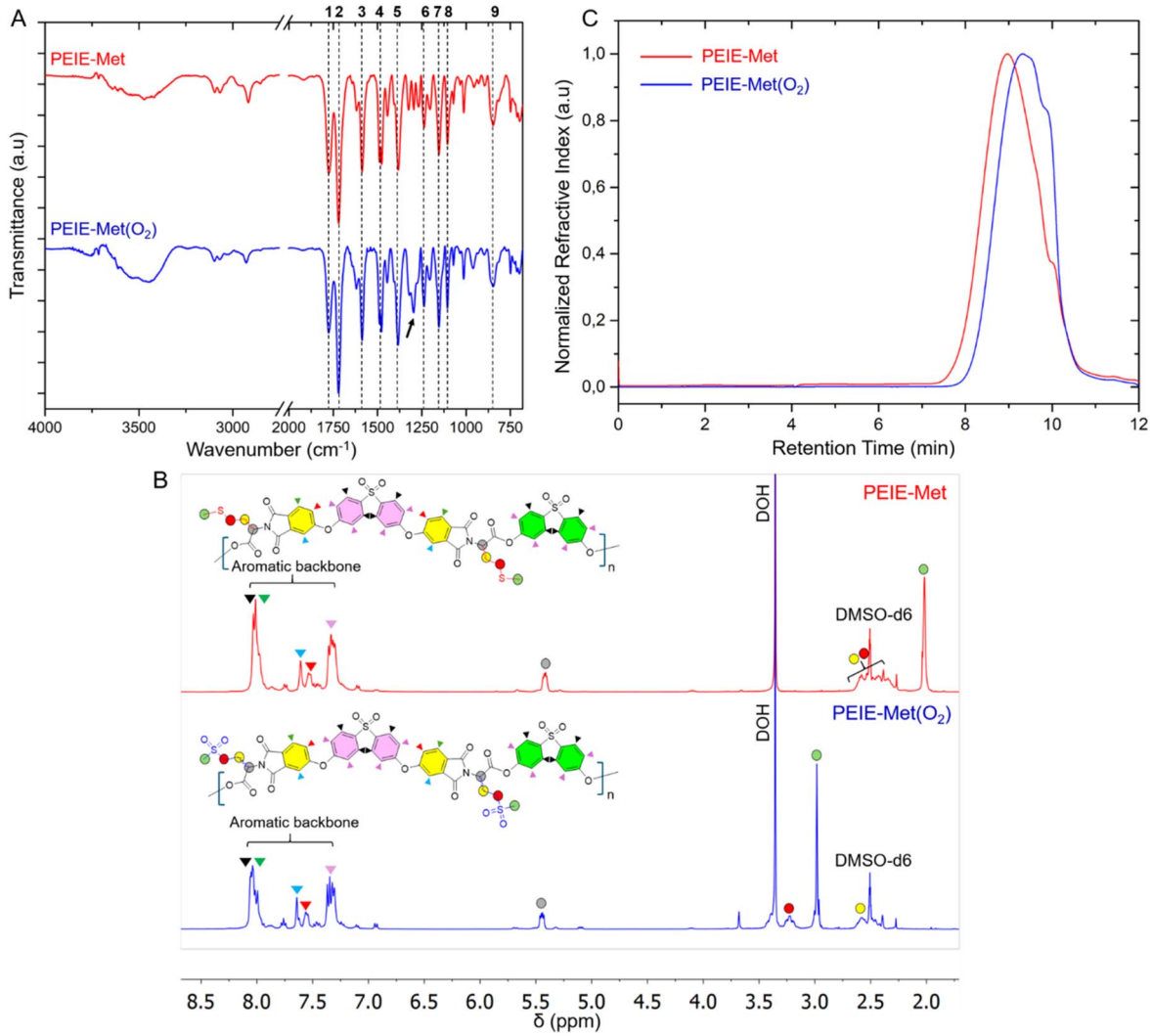

Fig. 1 FTIR spectra (A), ^{1}H-NMR spectra in DMSO-d_6 (B) and GPC traces (C) of PEIE-Met (red) and PEIE-Met(O_2) (blue).

Additionally, the band labeled 9, appearing at ~848 cm^{-1}, was previously related to the vibrational motions of *p*-substituted aromatic rings in PEIE systems. Sulfones are notable for exhibiting two well-known IR active signals ascribed to their symmetrical (1160–1120 cm^{-1}) and asymmetrical (1350–1300 cm^{-1}) S–O stretching motions.[38,48] In this context, since both polymers have at least two aromatic sulfones per monomer unit, the sharp signal centered at 1153 cm^{-1} (7) is associated with the symmetric vibrations of these entities, confirming their presence. Furthermore, analysis of the asymmetric stretching motions revealed one of the most notable differences between the spectra: a signal at 1300 cm^{-1}, highlighted by a black arrow in the PEIE-Met(O_2) spectrum. This suggests that the additional non-aromatic sulfone in PEIE-Met(O_2) may increase the intensity of the bands assigned to its asymmetric vibrations.

^{1}H and ^{13}C-NMR were also used to confirm the chemical structure of the designed PEIEs, complementing the above FTIR analysis. Fig. 1B displays the proton spectra of both samples, showing the complete and successful assignment of the different signals recorded for PEIE-Met and PEIE-Met(O_2). As previously stated, a remarkable similarity between the spectra was expected, particularly regarding the signal assignment of the protons that are part of the main chain. In this context, the signal pattern observed between 8.20 and 7.31 ppm, exhibiting a high degree of overlap, arises from protons belonging to the aromatic fragments (indicated with colored triangles), whereas the signal at 5.43 ppm (gray circle) indicates the presence of the proton attached to the α-carbon of amino acid residues. Conversely, the group of signals that differ most in terms of chemical shift originates from protons attached to the carbon atoms in the pendant groups of PEIE-Met and PEIE-Met(O_2). This can be attributed to the stronger inductive effect that sulfones exert on their neighboring atoms than thioethers do. Thus, it is evident that the methylene (red circle) and methyl (green circle) protons directly attached to thioether units experience a marked downfield shift when replaced by sulfones. For instance, while the S–CH_3 protons in PEIE-Met are positioned at 2.02 ppm, the S(O_2)–CH_3 protons in PEIE-Met(O_2) are shifted to 2.98 ppm. Additionally, ^{13}C-NMR analysis enables the identification of various signals that correlate well with the different

carbon nuclei present in both polymer structures (Fig. S10). Again, both spectra proved to be quite similar, with the main difference observed in the region of C atoms close to the thioether and sulfone groups. Unfortunately, in the case of PEIE-Met(O_2), signals attributed to C atoms directly attached to sulfone groups fall within the solvent signal region, affecting their visualization but confirming their presence by disrupting the symmetry of the DMSO-d_6 signal. Finally, GPC traces of the obtained systems are presented in Fig. 1C, from which their average molecular weights and dispersity ($Đ$) values were calculated. The number-average molecular weights (M_n) of PEIE-Met and PEIE-Met(O_2) were determined to be 6.6×10^3 and 3.5×10^3 g mol^{-1}, with $Đ$ values of 3.4 and 2.4, respectively. In this context, after considering the calculated M_n values and the molecular weights of the respective monomer units, both samples fall within the definition of oligomeric species. These results align well with previous reports employing the Higashi method for the preparation of polycondensates, although several reports convey such information on the basis of viscosity measurements.[39,41–43] Following the completion of the structural characterization, the thermal properties of both samples were evaluated *via* TGA and DSC analyses, and the results are shown in Fig. 2.

The TGA thermograms of the PEIEs are presented in Fig. 2A and B, alongside their derivative curves (DTGA, dashed lines). The recorded thermal profiles indicate that both specimens degrade in a very similar manner, exhibiting a primary degradation stage (referred to as T_{MD}) accompanied by two minor processes occurring at lower and higher temperatures. These T_{MD} stages are centered at approximately 389 °C and 387 °C for PEIE-Met and PEIE-Met(O_2), respectively, accounting for more than 85% of the degradable mass, in addition to the remaining pyrolytic residues, which range between 25% and 30% for both samples. Given that both materials possess nearly identical chemical structures and exhibit highly similar TGA thermograms, with T_{MD} processes occurring within a comparable temperature range, it can be inferred that their degradation follows similar mechanisms. However, it is essential to note the high diversity of chemical bonds, encompassing a variety of atom combinations in the main chain involving C, N, O, and S within both aliphatic and aromatic structures. The fact that most of the sample mass is volatilized in a single primary stage, spanning at least 200 °C, suggests that the degradation of these PEIEs is a complex process. In this context, it is anticipated that a combination of overlapping events on the temperature scale would take place, likely resulting in a random fragmentation

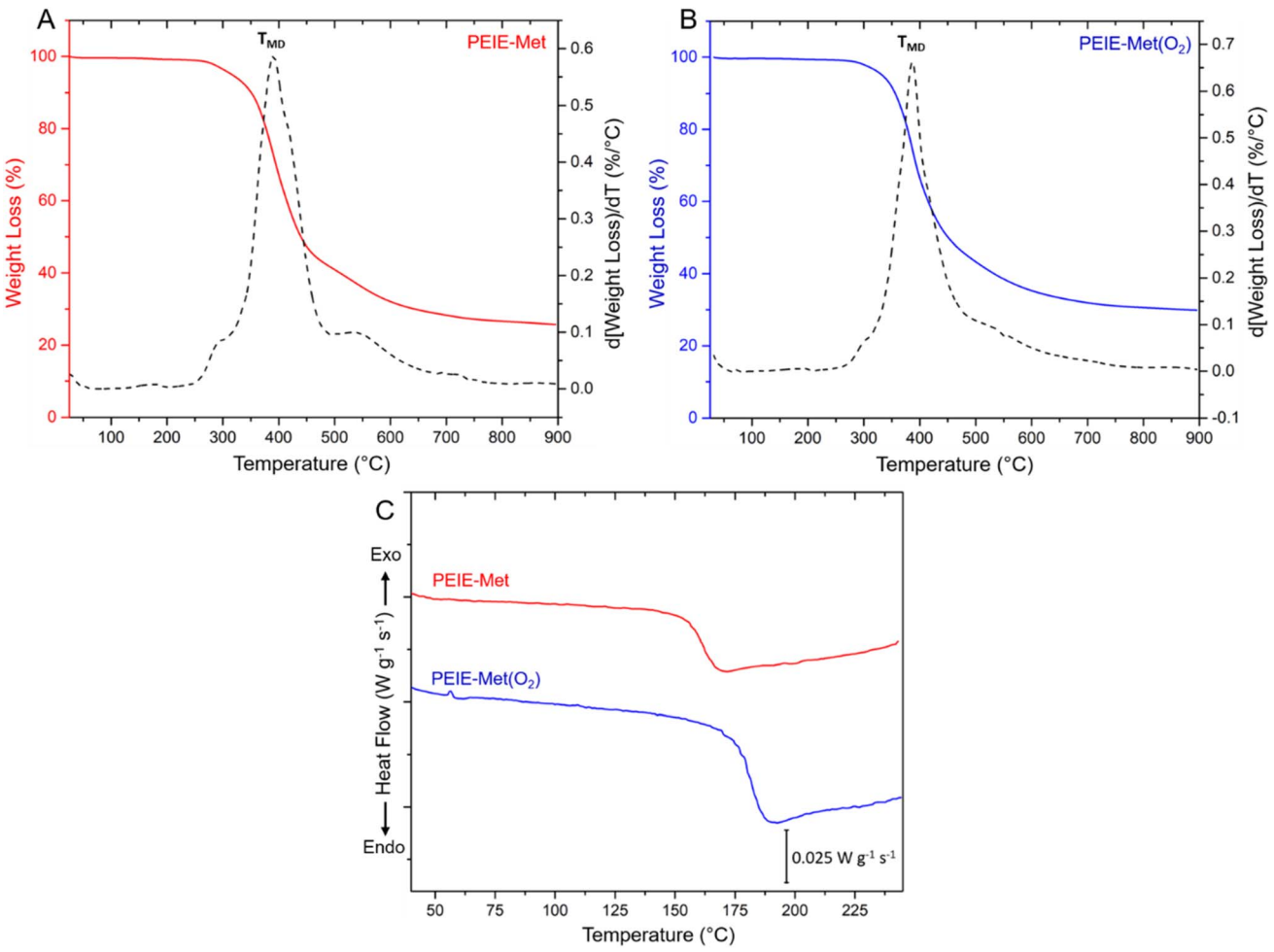

Fig. 2 TGA and DTGA thermograms of PEIE-Met (A) and PEIE-Met(O_2) (B). DSC traces from the final heating cycle recorded for both PEIEs (C).

mechanism initiated by the scission of the most strained and labile linkages. More importantly, from the perspective of potential applications, both samples presented T_i values exceeding 300 °C, specifically 325 °C and 338 °C for PEIE-Met and PEIE-Met(O_2), respectively, surpassing the reference value of 250 °C, thus classifying them as high-thermal resistance materials suitable for most capacitor applications.[49] Regarding calorimetric analyses, Fig. 2C illustrates the recorded DSC thermograms, where the complete absence of melting-crystallization phenomena confirms the amorphous nature of PEIEs, meeting one of the criteria for classification as dipolar glass polymers. Furthermore, direct examination of the DSC traces revealed that their T_g values as distinct jumps in heat flow, indicating values of 162 °C and 182 °C for PEIE-Met and PEIE-Met(O_2), respectively. Notably, both values significantly exceed room temperature, as required to minimize the influence of dissipative phenomena in dielectric media. On the other hand, the higher T_g value observed for PEIE-Met(O_2) is particularly noteworthy, especially considering its lower M_n than that of PEIE-Met. This may be attributed to the additional sulfone group, which likely enhances interchain dipolar interactions within the bulk material, a phenomenon previously reported in polymers containing dipolar entities that is expected to reduce the segmental mobility of chains.[18,50]

The dielectric properties of the obtained materials were first addressed by analyzing their ε_r' and tan(δ) isochronal representations (Fig. 3), which illustrate how both parameters evolve with temperature at fixed frequencies. To our delight, both PEIEs can be classified as high-dielectric polymer materials, successfully meeting the $\varepsilon_r' > 5.0$ criterion and exhibiting ε_r' values exceeding 5.0 at temperatures as low as −150 °C (Fig. 3A and B).[2] At room temperature and 1 Hz, the ε_r' values for PEIE-Met and PEIE-Met(O_2) were 5.7 and 7.1, respectively. Given the close structural similarity between both samples, the higher ε_r' recorded for PEIE-Met(O_2) can be attributed to the additional sulfone group from the oxidized methionine residue. This structural modification enhances the ability of the material to achieve a higher polarized state through expected orientational

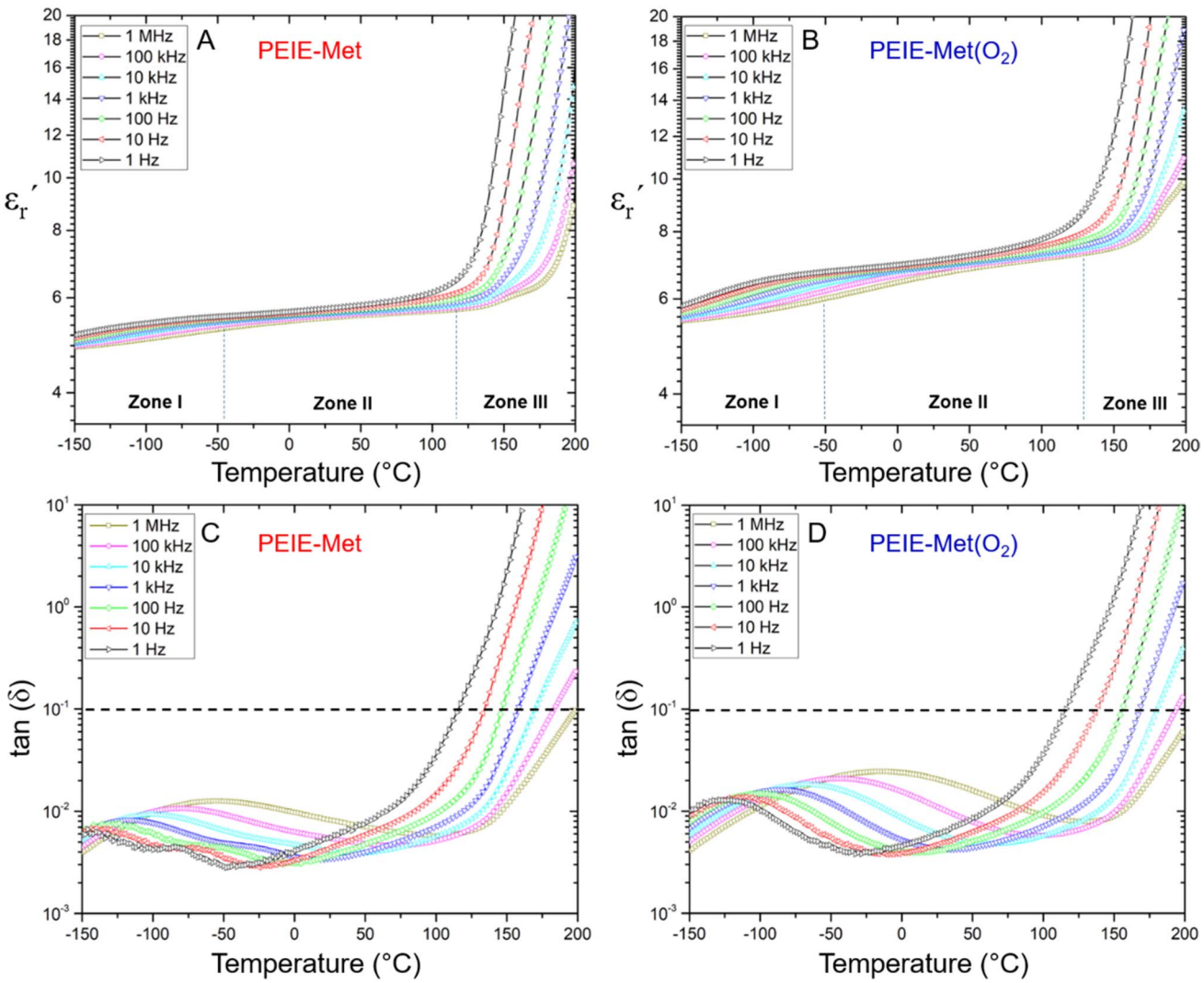

Fig. 3 ε_r' and tan(δ) isochronal curves for PEIE-Met (A and C) and PEIE-Met(O_2) (B and D).

motions, as will be further discussed. This result aligns well with previous reports highlighting the effectiveness of sulfone groups in enhancing dielectric properties, demonstrating that a slight modification in the monomer structure can lead to a significant increase in ε_r'.[13] Equally important is the value of tan(δ) displayed by both samples, which is a direct measurement of the dissipative behavior of the material. As shown in Fig. 3C and D, both PEIEs exhibit tan(δ) < 0.1 over a broad temperature range, surpassing this threshold only above 100 °C. At room temperature, tan(δ) values in the range of 0.003–0.005 and 0.004–0.006 were measured for PEIE-Met and PEIE-Met(O_2), respectively. To date, biaxially oriented polypropylene (BOPP) is considered the gold standard in terms of tan(δ) for polymer materials, with tan(δ) ≈ 0.0002.[51] However, these low values are partly due to the lack of relaxation phenomena due to the lack of dipolar entities in its structure. It is well established that incorporating dipolar structures to increase ε_r' typically leads to a higher tan(δ), necessitating a balance between both parameters.[52] In this context, Baer and Zhu classified high-dielectric polymers on the basis of their tan(δ) values, distinguishing between materials with low (<0.002) and ultralow (<0.005) loss factors.[2] Other reports consider materials with tan(δ) ≈ 0.02 as having reasonably low dissipation.[9] In view of the above, at room temperature, the obtained PEIEs would fit into the category of low dissipative materials, with tan(δ) values approaching the ultralow-loss regimen. The results obtained here allow these materials to be placed in a competitive position regarding some of our previous reported systems. Of particular interest result the comparison with those itaconate-based materials due to also their sustainable character. The results obtained in this study position the newly developed materials competitively with some of our previously reported systems. Of particular interest is the comparison with itaconate-based polymers, which also offer a sustainable alternative due to the bio-based origin of itaconic acid. For example, although polyitaconates PSO_2MeI and PCNMeI (ref. 18) exhibit slightly higher ε' values compared to PEIE-Met and PEIE-Met(O_2), the latter display a markedly lower dissipative character, as evidenced by tan(δ) values at least one order of magnitude lower. Furthermore, the significantly higher T_g values of the PEIEs enable them to maintain superior dielectric performance across a broader range of operating temperatures. Then, in two subsequent studies, we introduced bulky aliphatic groups into polyitaconate structures bearing sulfone and nitrile moieties, aiming to reduce their dissipative character by lowering tan(δ) and increasing T_g (ref. 20 and 21). However, this was achieved at the expense of significantly reduced ε' values, argued in terms of decreased dipolar density. In this context, the PEIEs developed in the present work clearly outperform these bulky polyitaconates by simultaneously exhibiting lower tan(δ), higher T_g values, and even higher ε'. Therefore, the strategy presented here represents a significant advancement in the design of efficient and sustainable dielectric materials. Table 1 summarizes the ε_r' and tan(δ) values recorded at room temperature for PEIE-Met and PEIE-Met(O_2).

Table 1 Dielectric constant (ε_r') and loss factor (tan(δ)) values of PEIE-Met and PEIE-Met(O_2) recorded at room temperature

	ε_r'(1 Hz)	ε_r'(1 kHz)	tan(δ) (1 Hz)	tan(δ) (1 kHz)
PEIE-Met	5.7	5.6	0.005	0.003
PEIE-Met(O_2)	7.1	6.9	0.006	0.004

A more detailed analysis of Fig. 3A and B allows the identification of three marked zones where ε_r' behaves differently with temperature. Zone I is delimited between −150 °C and −50 °C, where both PEIEs exhibit a first jump in their ε_r' values, which is more pronounced for PEIE-Met(O_2). Owing to these jumps, the ε_r' values increase (*e.g.*, at 1 Hz) from 5.1 to 5.5 and from 5.7 to 6.7 for PEIE-Met and PEIE-Met(O_2), respectively. Zone II (−50 °C to ∼100 °C) shows a gradual, steady increase in ε_r', whereas Zone III (>100 °C) is marked by a sharp rise, indicating the transition to the paraelectric state. According to previous studies, Zones I and II represent the dipolar glass polymer regime, where polarization is governed primarily by local orientational motions of discrete dipole structures.[18] As the temperature nears or exceeds the T_g (Zone III), the activation of long-segmental motions typical of the rubbery state enables achieving the paraelectric state, characterized by an abrupt increase in ε_r', ε_r'' and tan(δ), driven by polymer chain mobility and ionic conductivity from diffusing ionic impurities.[9] This highly polarized yet highly dissipative state is explained by the translational motions of the polymer chains, which begin to contribute to the existing local motions of dipoles.[26] Thus, on the one hand, the increased polarization should be attributed to the larger proportion of dipoles that can now participate in the material's polarization due to the reduction in the steric restrictions imposed by the vitreous state. On the other hand, these same chain motions also enhance molecular friction and ionic conductivity, amplifying the dissipative character of the material. To determine the optimal working temperature range, the $T_{paraelectric}$ (temperature at which the paraelectric state begins) was estimated *via* previously reported protocols and ε_r' isochronal representations at 1 Hz.[27] The calculated $T_{paraelectric}$ values were 137 °C for PEIE-Met and 152 °C for PEIE-Met(O_2). As expected, the higher $T_{paraelectric}$ of PEIE-Met(O_2) correlates with its higher T_g, which delays the onset of dissipative phenomena. This property extends the operational temperature range where these materials can work optimally by exhibiting a polarized state while minimizing energy dissipation.

The behavior of ε_r' through the different zones can be well correlated with various relaxation and dissipative phenomena observed during the analysis of the dielectric loss (ε_r'') isochrones presented in Fig. 4A and B. However, to facilitate the discussion of the relaxations observed in these systems, Fig. 4C groups the ε_r'' isochrones of both samples recorded at 10 Hz. Overall, these figures reveal that PEIE-Met and PEIE-Met(O_2) present similar spectra dominated by relaxation processes in the low-, medium- and high-temperature regimens. Relaxations occurring at temperatures below T_g (sub-T_g transitions) are typically attributed to local motions of dipolar entities constrained by a distribution of potential energy barriers provided by the glassy matrix.[52] Since both PEIE samples have almost identical chemical structures, similar dielectric responses

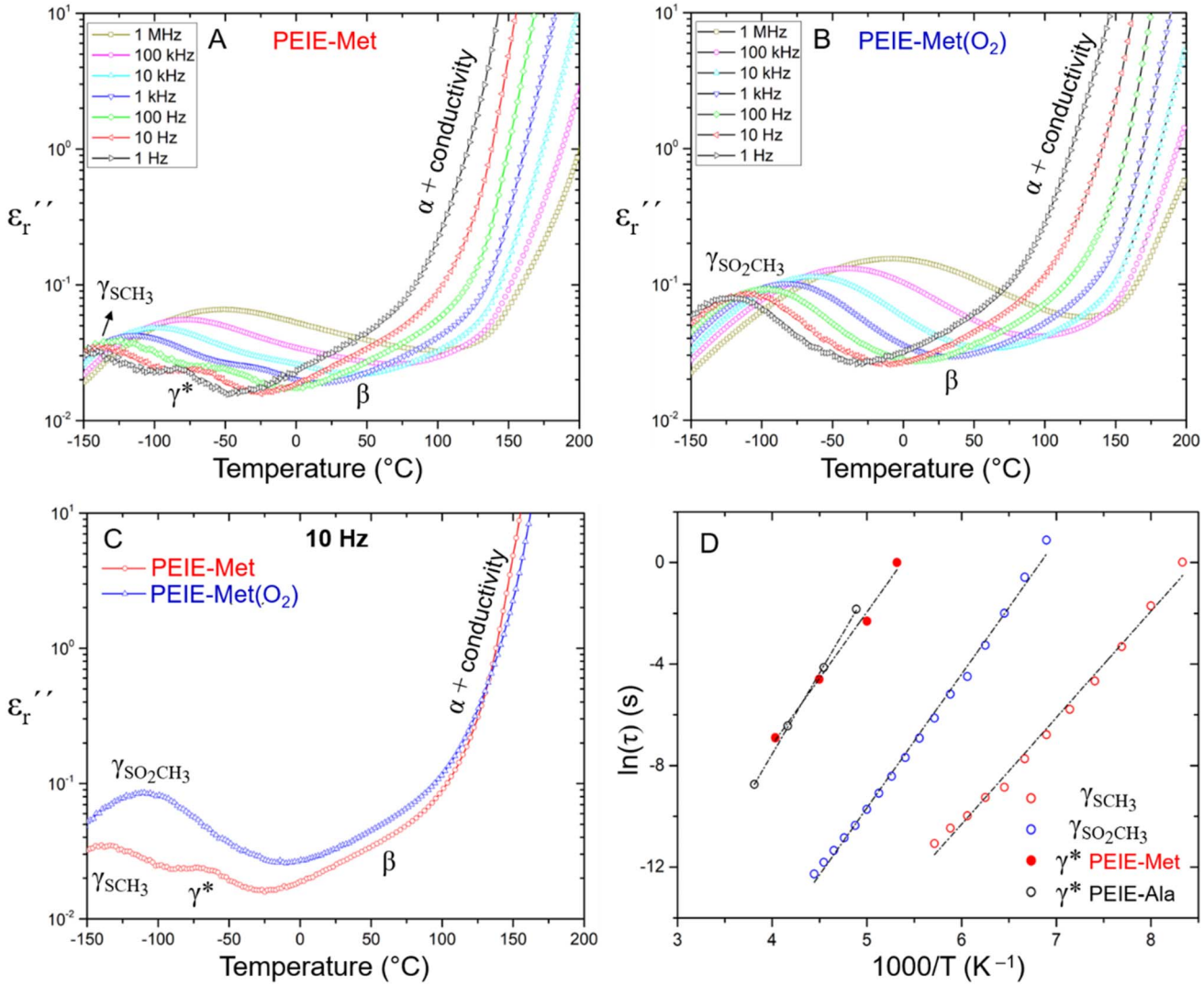

Fig. 4 ε_r'' isochronal representations for PEIE-Met (A) and PEIE-Met(O_2) (B). ε_r'' isochrones recorded at 10 Hz (C) and the relaxation map (D) of the low-temperature transitions detected in the PEIE samples.

across different temperature ranges are expected. However, most dipoles present in these PEIEs (*e.g.*, aromatic sulfones and carbonyls from imide and ester functionalities) are integrated into the aromatic main chains. Consequently, their movements are expected to be more restricted and require higher activation temperatures than those of the aliphatic thioether and sulfone units connected to the amino acid fragments. Indeed, several reports on polymers with aliphatic sulfones similar to those in our PEIEs indicate that dielectric relaxations are linked to their orientational motions occurring at temperatures as low as −100 °C. In our case, Fig. 4C reveals active relaxations for both samples in the low-temperature regime (from −150 °C to −50 °C), a region where their behaviors differ the most. Notably, PEIE-Met exhibits two slightly overlapped but distinct processes labeled γ_{SCH_3} and γ^*, while the isochrone recorded for PEIE-Met(O_2) initially appears to indicate a single transition, $\gamma_{SO_2CH_3}$, emerging within the same temperature range but exhibiting higher dielectric strength. Nevertheless, a closer inspection of $\gamma_{SO_2CH_3}$ suggests the presence of a hidden γ^*-like transition, which is overshadowed by the high-temperature tail of $\gamma_{SO_2CH_3}$. At 10 Hz, γ_{SCH_3} and γ^* appear centered at −137 °C and −70 °C, respectively, whereas $\gamma_{SO_2CH_3}$ is centered at −111 °C.

These results confirm the significant role of γ_{SCH_3} and $\gamma_{SO_2CH_3}$ in governing polarization at very low temperatures, enabling higher ε_r' values. As their labels suggest, we hypothesize that these relaxations likely originate from orientational motions of the amino acid pendant groups. To test this hypothesis, we prepared a third PEIE (PEIE-Ala) using alanine instead of methionine or methionine sulfone. The dielectric characterization of PEIE-Ala is shown in Fig. S11. The ε_r'' profiles recorded for PEIE-Ala revealed the absence of any relaxation below −100 °C, confirming our hypothesis regarding the origins of γ_{SCH_3} and $\gamma_{SO_2CH_3}$. Interestingly, PEIE-Ala exhibits a clear transition centered at −69 °C (1 Hz), matching properly with the features shown by the γ^* relaxation detected in PEIE-Met and possibly present in PEIE-Met(O_2). Given that PEIE-Ala lacks dipolar pendant groups, this relaxation likely arises from backbone-related dipolar entities. Although assigning γ^* to

a specific structure is complex and beyond the scope of this study, prior reports associated similar relaxations with the orientational motions of carbonyl species from ester linkages, which experience less hindrance than aromatic sulfones and imides.[53] Furthermore, the behavior of ε_r'' between 0 °C and 100 °C, before being influenced by conductivity effects, suggests that the activation of molecular motions requires higher temperatures, likely due to their more impeded nature. These motions, grouped as β transitions, align with reported dynamics of aromatic sulfones within polymer structures, giving rise to relaxations with similar characteristics linked to non-local motions caused by packing defects.[54] To provide a clearer description of these dielectric relaxations, Fig. 4D presents a relaxation map illustrating the temperature dependence of the relaxation times (τ) associated with the transitions observed in these samples. Data were extracted from ε_r'' isotherm curves recorded over a 10^{-1}–10^{5} Hz frequency range (Fig. S12). The inverse frequency value ($1/f = \tau$) at each isotherm peak was plotted as $\ln(\tau)$ *versus* the inverse of the temperature. This type of data representation can be adapted to the Arrhenius formalism through linear fittings that facilitate the calculation of key parameters such as the activation energies (E_a) of molecular motions.[55] On this basis, an initial comparison of γ_{SCH_3} and $\gamma_{SO_2CH_3}$ confirms that the former is activated at lower temperatures, which is consistent with prior ε_r'' isochrone analysis. Moreover, their distinct linear fit slopes indicate variations in E_a values, which are linked to different potential energy barriers associated with their molecular motions. The E_a values calculated for γ_{SCH_3} and $\gamma_{SO_2CH_3}$ are 34.9 and 43.8 kJ mol^{-1}, respectively, confirming that sulfones must overcome a higher potential energy barrier than thioether units to pursue orientational motion. The higher E_a calculated for sulfones could be attributed to stronger dipolar interactions – due to their greater dipole moment – that these entities might exert with their chemical surroundings. This energy requirement, supplied through thermal energy, explains why thioethers exhibit shorter relaxation times than sulfones at the same temperature. However, the E_a values measured here remain significantly lower than those reported for other systems.[9,18,21] Finally, the γ^* relaxations in PEIE-Met and PEIE-Ala exhibit similar temperature-dependent relaxation times, reinforcing their origin from backbone dipolar structures. The slight variation in slope between both specimens likely stems from structural differences within the polymeric matrix, influenced by the differing amino acid residues.

To achieve a more device-relevant characterization, the discharged energy density (U_e) and discharge efficiency (η) of capacitor-like configurations were determined from unipolar *P*–

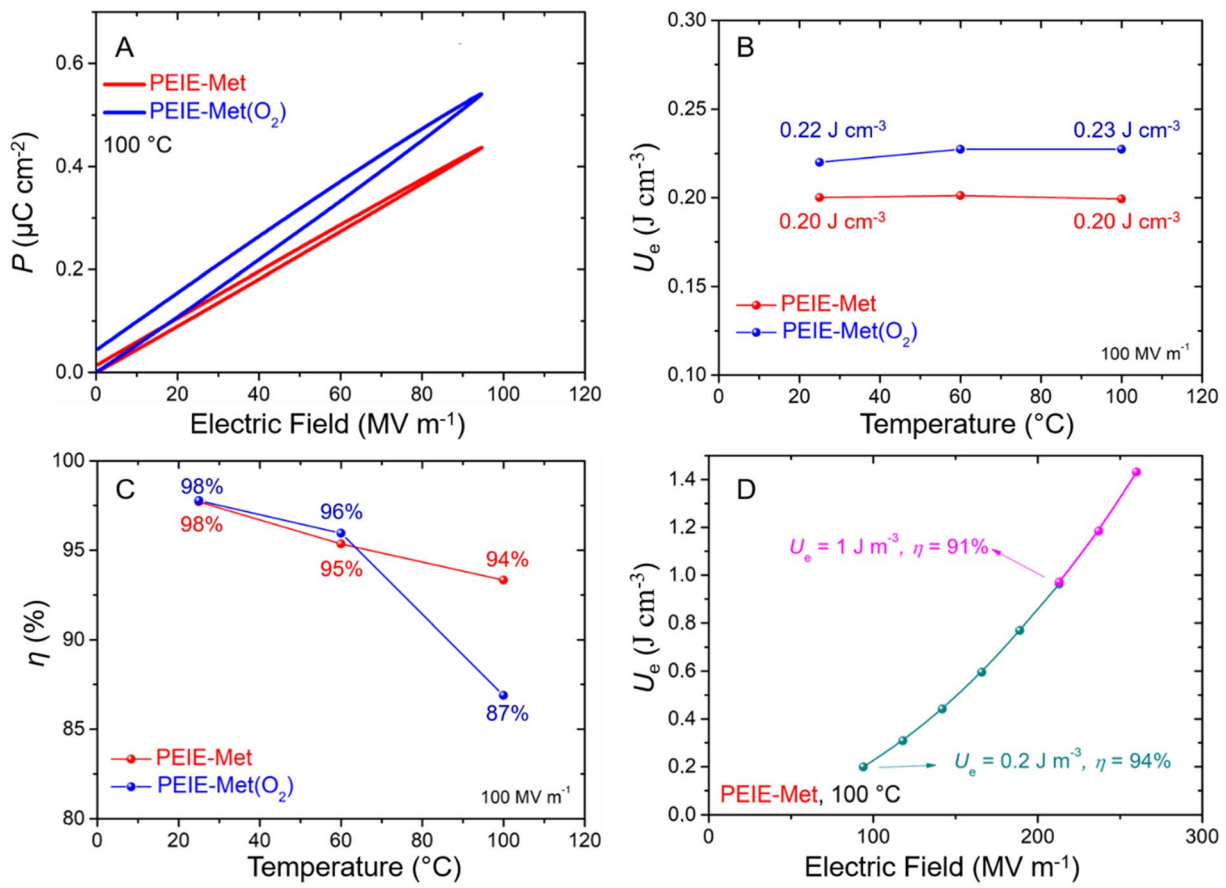

Fig. 5 (A) Unipolar *P*–*E* loops recorded at 100 °C for PEIE-Met and PEIE-Met(O_2). (B) Discharged energy density (U_e) and (C) discharge efficiency (η) as a function of temperature, measured at 100 MV m^{-1}. (D) Relationship between U_e and electric field for PEIE-Met at 100 °C. In all measurements, the electric field oscillation was maintained at a fixed frequency of 100 Hz.

E loop experiments (Fig. 5A). These measurements provide insight into the behavior of dielectric materials under realistic operating conditions, addressing charge and discharge processes at elevated temperatures and voltages. Fig. 5A presents the *P–E* loops for both PEIEs, recorded at 100 °C over an electric field range from 0 to 100 MV m^{-1}. The first notable observation is that the loop for PEIE-Met(O_2) exhibits a steeper slope than that of PEIE-Met, consistent with the higher ε_r' value of the former. According to eqn (2), this increased slope, resulting from a higher ε_r', directly correlates with greater U_e, as confirmed by Fig. 5B. The data in Fig. 5B show that at 100 MV m^{-1} and three different temperatures (25, 60, and 100 °C), U_e values were higher for PEIE-Met(O_2) (0.22–0.23 J cm^{-3}) compared to PEIE-Met (0.20 J cm^{-3}). Despite this, it is important to note that the U_e values achieved by PEIE-Met(O_2) were not significantly higher than those of PEIE-Met. This may be attributed to the more pronounced hysteresis observed in the *P–E* loops (Fig. 5A). This observation is crucial, as hysteresis directly reflects the energy lost during the charge–discharge process.[6] At 100 °C and 100 MV m^{-1}, PEIE-Met(O_2) exhibits a more dissipative behavior than PEIE-Met. Consequently, despite its lower ε_r', the latter functions as a more efficient energy storage material under these conditions. To quantitatively support the above, η values for both PEIEs are presented in Fig. 5C. As expected, at 100 °C, η values of 94% and 87% were calculated for PEIE-Met and PEIE-Met(O_2), respectively, confirming the superior performance of the former. However, as the temperature decreased, η values above 95% were recorded for both samples, highlighting their excellent energy storage properties. Notably, at 60 °C, the trend is reversed, with PEIE-Met(O_2) achieving a higher η (96%) than PEIE-Met (95%), while at room temperature, both materials exhibited η values of 98%. In all cases, the recorded η values remained above the 80% threshold, demonstrating their suitability for energy storage applications.[56] Based on previous reports, the greater hysteresis observed in PEIE-Met(O_2) could be attributed, among other dissipative phenomena, to the more intense relaxation processes of sulfone groups, which lead to higher dielectric losses.[57] Moreover, it is important to consider that the thickness of samples is a crucial factor when studying dielectric properties at high voltages, with more reliable results obtained with slightly thicker films, as thicknesses near 1 μm are especially unforgiving to defects during film fabrication, leading to higher conduction losses or early breakdown of the capacitors. A thickness ~5 μm has proven more reliable in circumventing these limitations while remaining low enough to have a high capacitance and reach high electric fields with moderate voltages. Thus, although the efficiency drops for the PEIE-Met(O_2), its higher permittivity is encouraging, and better performance could certainly be achieved with other techniques that allow the production of samples with a more optimal thickness range (*e.g.*, multilayer samples produced with blade-coating). Subsequently, driven by the superior and more stable performance of PEIE-Met, we aimed to explore its behavior at higher electric fields. Using data extracted from *P–E* loop measurements conducted at 100 °C (Fig. S13), we obtained U_e values at electric fields exceeding 100 MV m^{-1} (Fig. 5D). Notably, the sample registered an increase of U_e, going from 0.2 J cm^{-3} (at 100 MV m^{-1}) to 1.0 J cm^{-3} (at 200 MV m^{-1}), accompanied by a minimum reduction of η (from 94 to 91%). Therefore, by maintaining efficiency values above 90% at high temperatures and voltages, PEIE-Met can be regarded as a promising dielectric material for energy storage applications, matching some of the best-performing linear dielectrics, such as BOOP and other dipolar glasses.[56]

4. Conclusions

In this study, we successfully synthesized and characterized two novel poly(ether-imide-ester) (PEIE) polymers incorporating methionine (PEIE-Met) and its oxidized form, methionine sulfone (PEIE-Met(O_2)), as dipolar pendant units. Structural analysis *via* FTIR, NMR, and GPC confirmed the successful incorporation of these amino acid residues, whereas TGA and DSC measurements demonstrated their excellent thermal stability, with onset degradation temperatures above 300 °C and T_g values of 162 °C and 182 °C for PEIE-Met and PEIE-Met(O_2), respectively. Broadband dielectric spectroscopy revealed that both polymers exhibit high dielectric constants ($\varepsilon_r' > 5.0$) and low dielectric losses ($\tan(\delta) < 0.01$) over a broad range of temperatures, making them promising candidates for high-dielectric applications. Notably, at room temperature, PEIE-Met(O_2) displayed a greater ε_r' (7.1 at 1 Hz) than did PEIE-Met (5.7 at 1 Hz), which can be attributed to the increased dipole moment of the sulfone groups. Additionally, their paraelectric transition temperatures ($T_{paraelectric}$) were determined to be 137 °C and 152 °C, respectively, suggesting that PEIE-Met(O_2) can sustain a polarized state over a wider temperature range before exhibiting significant energy dissipation. Dielectric loss analysis (ε_r'' isochrones) revealed multiple relaxation processes, including those involving γ_{SCH_3} and $\gamma_{SO_2CH_3}$, which govern the polarization of these samples from low temperatures. A comparative study using an alanine-based polymer (PEIE-Ala) confirmed that these relaxations originate from the amino acid pendant groups. Subsequently, *P–E* loop measurements enabled a device-relevant characterization, confirming that both specimens achieved discharge efficiency values above 85% under high-temperature and high-voltage conditions. Particularly noteworthy were the results obtained with PEIE-Met, which demonstrated efficiencies exceeding 90% at 100 °C and electric fields up to 200 MV m^{-1}, highlighting the suitability of these materials as dielectric layers for energy storage applications. Overall, our findings highlight the potential of bio-derived entities as viable building blocks for high-performance dielectric materials, paving the way toward more sustainable technologies by reducing reliance on fossil-based resources while maintaining, or even enhancing, functional properties. By leveraging the high dipole moment of sulfone groups and the intrinsic thermal stability of PEIEs, we present a more sustainable and scalable strategy for the design of next-generation polymer dielectrics. We acknowledge that the chemical design of our systems still relies in part on petroleum-derived fragments. However, the success of this initial approach provides both the motivation to continue progressing in this

direction and, we hope, the inspiration for other researchers to pursue and explore similar strategies toward more sustainable dielectric materials.

Author contributions

S. B.: conceptualization, data curation, formal analysis, investigation, methodology, writing – original draft, writing – review & editing. M. B.: investigation. F. G.: investigation. S. Z.: data curation, investigation. F. L. G.: data curation, investigation, formal analysis. D. D. D.: resources, funding acquisition, writing – review & editing, J. P.: writing – review & editing, J. M.: data curation, formal analysis, funding acquisition, writing – review & editing.

Conflicts of interest

The authors declare that they have not competing financial interests or personal relationships that could have appeared to influence the work reported in this study.

Data availability

The data supporting this article have been included as part of the SI. Access to any additional information would be available from the corresponding authors under request. Supplementary information is available. See DOI: **https://doi.org/10.1039/d5ta02785c**.

Acknowledgements

S. B., J. A. P. and J. M. acknowledge grant no. TED2021-130107A-I00 funded by MICIU/AEI/10.13039/501100011033 and "European Union NextGenerationEU/PRTR, the grant PID2021-123438NB-I00 funded by MCIN/AEI/10.13039/501100011033 and by ERDF A way of making Europe and the grant IT-1566-22 from Eusko Jaurlaritza (Basque Government). S. B. and J. M. are also thankful for the financial support from Gipuzkoako Foru Aldundia through the Programa de Red Guipuzcoana de Ciencia, Tecnología e Innovación (code: 2023-CIEN-000069-01). J. M. acknowledges support from the "Ramon y Cajal" Program, grant no. RYC2023-044285-I, funded by MICIU/AEI/10.13039/501100011033 and ESF+. S. Z. and F. L. G. acknowledge the financial support from the Industrial Chair SMILE within the grant agreement no. ANR-19-CHIN-0002 and the Equipex ELORPrintTec ANR-10-EQPX-28-01 with the help of the French State's Initiative d'Excellence IdEx ANR-10-IDEX-003-02. D. D. D. acknowledge Cátedra Fundación CEPSA of the ULL, Cátedra de Medioambiente y Sostenibilidad (Cabildo de Tenerife-ULL), Fundación Ramón Areces and the Ministry of Science and Innovation (project PID2022-142118OB-I00/AE/10.13039/501100011033/UE) for financial support, and Nanotec, INTech, Cabildo de Tenerife and ULL for laboratory facilities. The authors express their gratitude to Chioma I. Aja for her assistance during part of the tasks related to synthesis and characterization analyses.

References

1 Q.-K. Feng, S.-L. Zhong, J.-Y. Pei, Y. Zhao, D.-L. Zhang, D.-F. Liu, Y.-X. Zhang and Z.-M. Dang, *Chem. Rev.*, 2021, **122**, 3820–3878.
2 E. Baer and L. Zhu, *Macromolecules*, 2017, **50**, 2239–2256.
3 S. Bonardd, V. Moreno-Serna, G. Kortaberria, D. Díaz Díaz, A. Leiva and C. Saldías, *Polymers*, 2019, **11**, 317.
4 H. Li, Y. Zhou, Y. Liu, L. Li, Y. Liu and Q. Wang, *Chem. Soc. Rev.*, 2021, **50**, 6369–6400.
5 Y. Qiao, X. Yin, T. Zhu, H. Li and C. Tang, *Prog. Polym. Sci.*, 2018, **80**, 153–162.
6 L. Zhu, *J. Phys. Chem. Lett.*, 2014, **5**, 3677–3687.
7 G. Zhang, Q. Li, E. Allahyarov, Y. Li and L. Zhu, *ACS Appl. Mater. Interfaces*, 2021, **13**, 37939–37960.
8 J. Chen, Z. Pei, B. Chai, P. Jiang, L. Ma, L. Zhu and X. Huang, *Adv. Mater.*, 2024, **36**, 2308670.
9 J. Wei, Z. Zhang, J.-K. Tseng, I. Treufeld, X. Liu, M. H. Litt and L. Zhu, *ACS Appl. Mater. Interfaces*, 2015, **7**, 5248–5257.
10 J. Wei, T. Ju, W. Huang, J. Song, N. Yan, F. Wang, A. Shen, Z. Li and L. Zhu, *Polymer*, 2019, **178**, 121688.
11 W. Huang, T. Ju, R. Li, Y. Duan, Y. Duan, J. Wei and L. Zhu, *Adv. Electron. Mater.*, 2023, **9**, 2200414.
12 D. Wu, X. Zhao, X. Li, J. Dong and Q. Zhang, *Polymer*, 2022, **256**, 125221.
13 Z. Zhang, D. H. Wang, M. H. Litt, L. S. Tan and L. Zhu, *Angew. Chem.*, 2018, **130**, 1544–1547.
14 Y.-F. Zhu, Z. Zhang, M. H. Litt and L. Zhu, *Macromolecules*, 2018, **51**, 6257–6266.
15 S. J. Dünki, E. Cuervo-Reyes and D. M. Opris, *Polym. Chem.*, 2017, **8**, 715–724.
16 Y. Sheima, T. R. Venkatesan, H. Frauenrath and D. M. Opris, *J. Mater. Chem. C*, 2023, **11**, 7367–7376.
17 Y. Liang, J. Xu, W. Sun, T. Li, C. Dong, Y. Zhou, H. Zheng, Y. Cheng and L. Zhang, *Chem. Eng. J.*, 2024, **484**, 149458.
18 S. Bonardd, A. Alegria, C. Saldias, A. Leiva and G. Kortaberria, *ACS Appl. Mater. Interfaces*, 2018, **10**, 38476–38492.
19 S. Bonardd, C. Saldías, Á. Leiva, D. Díaz Díaz and G. Kortaberria, *Polymers*, 2021, **13**, 317.
20 S. Bonardd, Á. Alegria, O. Ramirez, C. Saldías, Á. Leiva and G. Kortaberria, *React. Funct. Polym.*, 2019, **140**, 1–13.
21 S. Bonardd, J. Maiz, A. Alegría, J. A. Pomposo, E. V. Sesto, G. Kortaberria and D. D. Díaz, *React. Funct. Polym.*, 2024, **196**, 105842.
22 F. Owusu, M. Tress, F. A. Nüesch, S. Lehner and D. M. Opris, *Mater. Adv.*, 2022, **3**, 998–1006.
23 Y. Tang, W. Xu, S. Niu, Z. Zhang, Y. Zhang and Z. Jiang, *J. Mater. Chem. A*, 2021, **9**, 10000–10011.
24 Z. Zhang, J. Zheng, K. Premasiri, M.-H. Kwok, Q. Li, R. Li, S. Zhang, M. H. Litt, X. P. Gao and L. Zhu, *Mater. Horiz.*, 2020, **7**, 592–597.
25 Y. Duan, T. Wongwirat, T. Ju, S. Zhang, J. Wei and L. Zhu, *J. Mater. Chem. A*, 2023, **11**, 20021–20030.
26 S. Bonardd, Á. Alegría, J. Maiz and D. D. Díaz, *Mater. Today Chem.*, 2024, **40**, 102268.

27 S. Bonardd, Á. Alegría, C. Saldías, Á. Leiva and G. Kortaberria, *Polymer*, 2020, **203**, 122765.
28 R. Wang, Y. Zhu, J. Fu, M. Yang, Z. Ran, J. Li, M. Li, J. Hu, J. He and Q. Li, *Nat. Commun.*, 2023, **14**, 2406.
29 D. H. Wang, B. A. Kurish, I. Treufeld, L. Yang, L. Zhu and L.-S. Tan, *MRS Online Proc. Libr.*, 2013, **1541**, 10511.
30 Z. Li, X. Chen, C. Zhang, E. Baer, D. Langhe, M. Ponting, M. Brubaker, T. Hosking, R. Li and M. Fukuto, *ACS Appl. Polym. Mater.*, 2019, **1**, 867–875.
31 I. Treufeld, D. H. Wang, B. A. Kurish, L.-S. Tan and L. Zhu, *J. Mater. Chem. A*, 2014, **2**, 20683–20696.
32 D. H. Wang, B. A. Kurish, I. Treufeld, L. Zhu and L. S. Tan, *J. Polym. Sci., Part A: Polym. Chem.*, 2015, **53**, 422–436.
33 M.-H. Kwok, C. A. Bohannon, R. Li, B. Zhao and L. Zhu, *Giant*, 2021, **8**, 100079.
34 S. Cao, H. Tong, S. Wang and J. Liu, *Macromol. Rapid Commun.*, 2023, **44**, 2300372.
35 Q. Zhang, X. Chen, T. Zhang and Q. Zhang, *Nano Energy*, 2019, **64**, 103916.
36 S. Diaham and M.-L. Locatelli, *IEEE Trans. Dielectr. Electr. Insul.*, 2015, **22**, 3053–3058.
37 H. Ye, L. Chen, H. Jiang and L. Xu, *ACS Appl. Polym. Mater.*, 2024, **6**, 2524–2533.
38 A. J. Jose, R. Wilson, G. Jacob and M. Alagar, *Mater. Today: Proc.*, 2019, **9**, 279–294.
39 A. Tundidor-Camba, L. H. Tagle, C. A. Terraza, J. Rivera, D. Coll and P. A. Ortiz, *Polym. Bull.*, 2021, **78**, 4205–4225.
40 S. Mehdipour-Ataei and A. Amirshaghaghi, *J. Appl. Polym. Sci.*, 2005, **96**, 570–576.
41 S. Mallakpour and P. Asadi, *Colloid Polym. Sci.*, 2010, **288**, 1341–1349.
42 S. Mallakpour and H. Seyedjamali, *Amino Acids*, 2008, **34**, 531–538.
43 S. Mallakpour and E. Kowsari, *J. Appl. Polym. Sci.*, 2006, **101**, 455–460.
44 M. A. J. Mazumder, *Int. J. Electrochem. Sci.*, 2019, **14**, 1040–1068.
45 Q. He, K. Sun, Z. Shi, Y. Liu and R. Fan, *Mater. Today*, 2023, **68**, 298–333.
46 W. Chen, W. Chen, B. Zhang, S. Yang and C.-Y. Liu, *Polymer*, 2017, **109**, 205–215.
47 F. Higashi, N. Akiyama, I. Takahashi and T. Koyama, *J. Polym. Sci., Polym. Chem. Ed.*, 1984, **22**, 1653–1660.
48 S. Fujii and T. J. McCarthy, *Langmuir*, 2016, **32**, 765–771.
49 Q. Li, F.-Z. Yao, Y. Liu, G. Zhang, H. Wang and Q. Wang, *Annu. Rev. Mater. Res.*, 2018, **48**, 219–243.
50 J. T. Bendler, D. A. Boyles, C. A. Edmondson, T. Filipova, J. J. Fontanella, M. A. Westgate and M. Wintersgill, *Macromolecules*, 2013, **46**, 4024–4033.
51 C. Dervos, P. Tarantili and M. Athanassopoulou, *J. Phys. D: Appl. Phys.*, 2009, **42**, 135409.
52 C. C. Ku and R. Liepins, *Electrical Properties of Polymers*, Hanser publishers Munich, 1987.
53 J. de Abajo, J. G. de La Campa, A. Alegría and J. M. Echave, *J. Polym. Sci., Part B: Polym. Phys.*, 1997, **35**, 203–212.
54 J. Tsuwi, D. Pospiech, D. Jehnichen, L. Häußler and F. Kremer, *J. Appl. Polym. Sci.*, 2007, **105**, 201–207.
55 A. R. Blythe and D. Bloor, *Electrical Properties of Polymers*, Cambridge university press, 2005.
56 F. Le Goupil, V. Salvado, V. Rothan, T. Vidil, G. Fleury, H. Cramail and E. Grau, *J. Am. Chem. Soc.*, 2023, **145**, 4583–4588.
57 X. Li, T. Wongwirat, L. Li, Y. Xi, J. Wei and L. Zhu, *ACS Appl. Polym. Mater.*, 2025, **7**(5), 2965–2972.